De Michelis *et al. Earth, Planets and Space* (2016) 68:105
DOI 10.1186/s40623-016-0476-3

Earth, Planets and Space

FULL PAPER

Open Access

Observations of high-latitude geomagnetic field fluctuations during St. Patrick's Day storm: Swarm and SuperDARN measurements

Paola De Michelis[1*], Giuseppe Consolini[2], Roberta Tozzi[1] and Maria Federica Marcucci[2]

Abstract

The aim of this work is to study the properties of the magnetic field's fluctuations produced by ionospheric and magnetospheric electric currents during the St. Patrick's Day geomagnetic storm (17 March 2015). We analyse the scaling features of the external contribution to the horizontal geomagnetic field recorded simultaneously by the three satellites of the Swarm constellation during a period of 13 days (13–25 March 2015). We examine the different latitudinal structure of the geomagnetic field fluctuations and analyse the dynamical changes in the magnetic field scaling features during the development of the geomagnetic storm. Analysis reveals consistent patterns in the scaling properties of magnetic fluctuations and striking changes between the situation before the storm, during the main phase and recovery phase. We discuss these dynamical changes in relation to those of the overall ionospheric polar convection and potential structures as reconstructed using SuperDARN data. Our findings suggest that distinct turbulent regimes characterised the mesoscale magnetic field's fluctuations and that some factors, which are known to influence large-scale fluctuations, have also an influence on mesoscale fluctuations. The obtained results are an example of the capability of geomagnetic field fluctuations data to provide new insights about ionospheric dynamics and ionosphere–magnetosphere coupling. At the same time, these results could open doors for development of new applications where the dynamical changes in the scaling features of the magnetic fluctuations are used as local indicators of magnetospheric conditions.

Keywords: High-latitude phenomena, Solar wind–magnetosphere interactions, Ionospheric turbulence, Swarm magnetic measurements

Background

The Swarm mission (Olsen 2013) is set up to study the Earth's magnetic field and its temporal variations, as well as a variety of near-Earth environmental parameters. This European Space Agency (ESA) mission consists of three identical satellites making high-precision and high-resolution measurements of the strength, direction and variation of the geomagnetic field, complemented by precise navigation, accelerometer, plasma and electric field measurements. The Swarm constellation was launched on 22 November 2013, and after about a year and half on orbit, it provided a first magnetic measurement of the strongest geomagnetic storm of Solar Cycle 24. During this solar cycle, which began roughly on January 2008 and was characterised by a minimal activity until early 2010, there have been several moderate geomagnetic storms. Among them, the most severe geomagnetic storm occurred on St. Patrick's Day, 17 March 2015, with the arrival at Earth of a coronal mass ejection (CME) at 04:45 UT. The Nasa Advanced Composition Explorer (ACE) satellite, located at L1 Lagrangian point between the Earth and the Sun (about 1.5 million km forward of Earth along

*Correspondence: paola.demichelis@ingv.it
[1] Istituto Nazionale di Geofisica e Vulcanologia Roma, Via di Vigna Murata 605, 00143 Rome, Italy
Full list of author information is available at the end of the article

the Sun–Earth line), recorded changes in some important physical quantities such as the interplanetary magnetic field (IMF) and solar-plasma parameters which well describe both the arrival of the CME into the interplanetary medium and the interplanetary conditions that made possible the subsequent arrival of the disturbance at Earth. The St. Patrick's Day storm was characterised by a minimum value of the geomagnetic index *Sym-H* of −234 nT, realised on 17 March at 22:47 UT, and it produced a worldwide disturbance quantified by a value equal to 8 of the mid-latitude magnetic activity index *Kp*, which persisted for some hours during the main phase of the geomagnetic storm. As it is typical for a severe storm, during this event geomagnetic activity was particularly intense at high latitudes and auroral phenomena were observed even at surprisingly low latitudes around the globe. As reported by Cherniak and Zakharenkova (2015) and Nishitani et al. (2015) during the 17 March 2015 storm, auroral phenomena were observed even at very low magnetic latitudes in Europe, Japan and the USA.

For this reason, the St. Patrick's Day storm represents a good case study to investigate the changes in the features of the magnetic field fluctuations recorded by the magnetometers onboard the three Swarm satellites and produced by ionospheric and magnetospheric currents activated during the storm. These magnetic fluctuations as well as the fluctuations of other important physical parameters describing the magnetosphere–ionosphere system are expected to be characterised by a probability distribution or a power spectrum with no characteristic scale. This scale-free structure has been found analysing both the spectrum and the structure function of the ground magnetic field (Abel and Freeman 2002; Consolini et al. 1998; Pulkkinen et al. 2006), the ionospheric electric field spectrum (Abel and Freeman 2002; Golovchanskaya et al. 2006; Golovchanskaya and Kozelov 2010) and the structure functions of both ionospheric convection velocities (Abel et al. 2006; Parkinson 2006) and several geomagnetic indices (AE, AU, AL and PC). In situ measurements below 1000 km altitude have established that also the plasma density irregularities from scale lengths of 100 km to a few metres have power law spectra. Their origin is the result of a complex process part of which can be ascribed to turbulent processes (Dyson et al. 1974; Kelley et al. 1982). The feature of a scale-free structure for fluctuations in the magnetosphere–ionosphere system suggests that different physical processes both internal and external to the system may play an important role. An hypothesis is that these scale-free structures can originate from the scale-free nature characterising the solar wind and/or from some processes activated within the magntosphere–ionosphere system such as the magnetohydrodynamic turbulence (Borovsky and Funsten 2003) or self-organised criticality (Consolini 1997; Uritsky and Pudovkin 1998; Sitnov et al. 2001; Consolini and Chang 2001). In detail, the magnetic fluctuations are characterised by spectral features depending on latitude and geomagnetic activity level and by distinct turbulent regimes at various altitudes over the polar regions (Golovchanskaya et al. 2006; De Michelis et al. 2015). The turbulent character found in these regions may have multiple origins. Some theories relate the turbulence directly to turbulence in the solar wind, and others associate it with structures of magnetospheric origin, suggesting that it can be a consequence of a strong shear flow regime, of a strong gradient drift and/or of a current convective regime (Kintner and Seyler 1985). However, the emergence of these turbulence regimes is related to the enhancement of plasma density irregularities and to the development of the Kelvin–Helmoholtz instability. Thus, the ionospheric irregularities of magnetic origin are closely related to the plasma density irregularities that are due to the enhancement of particle precipitation in the auroral oval, to the variation of the ionospheric electric field and to the consequent intensification of the electric current systems. These ionospheric irregularities play an important role in the study of the ionosphere–magnetosphere coupling, and in a more practical framework, they are related to the conditions of the radio wave propagation in the ionosphere. The plasma density irregularities are, for example, the biggest error source for global positioning system (GPS) signals during space weather events by causing a decrease in the operational performance of navigation systems (Forte and Radicella 2004). Usually, these irregularities are studied considering the rate of total electron content index (ROTI) which detects them by measuring the irregular structure of the spatial gradient of the total electron content (TEC) (Pi et al. 1997) and is used to estimate the fluctuation activity and the auroral oval evolution (Cherniak et al. 2015). An interesting example of the application of this index to the study of the dynamics of the ionospheric irregularities during the St. Patrick's Day storm has been recently published by Cherniak et al. (2015). In this study, the authors, using data coming from more than 2500 ground-based GPS stations, reconstruct diurnal and hourly ROTI maps for both hemispheres showing the existence of a strong correlation between the ionospheric irregularities and the auroral hemispheric power (HP) index. This gives an estimate of the power in gigawatts of precipitating energetic particles in the polar regions. They find that the ionospheric irregularities increase within the polar cap region during the occurrence of the geomagnetic storm and that the spatial–temporal structure of the ionospheric irregularities between the two hemisphere is asymmetric.

In this work, we try to get information about the turbulent nature of the ionospheric plasma at high latitude by analysing the dynamical changes in the scaling features of small-scale fluctuations (less than 1 min) of the magnetic field recorded onboard of the Swarm satellites during the St. Patrick's Day geomagnetic storm of March 2015. As a matter of fact, the spatial features of the magnetic field fluctuations can be properly investigated using the Swarm measurements due to their high spatial resolution of about 7.6 km along the orbital track. We analyse the changes in the scaling properties of the horizontal intensity of the geomagnetic field's spatial fluctuations. To do this, we evaluate the local Hurst exponent, which characterises the fluctuations observed in a signal defining their degree of persistence or anti-persistence. We compare the observed changes to those of the overall ionospheric polar convection and potential structures as reconstructed using data from observations made by the Super Dual Auroral Radar Network (SuperDARN). We want to test the possibility to utilise the changes in statistical parameters as a local indicator of overall magnetospheric–ionospheric coupling conditions.

The paper is organised as follows. At first, the data sources are discussed, and then, a brief summary of the method of analysis is presented. Following this, the analysis is applied on the selected data. Finally, the implications of findings are discussed.

Data

We consider low resolution (1 Hz) magnetic data recorded onboard of the ESA Swarm mission from 13 to 25 March 2015. The magnetic field data are vector magnetic measurements recorded simultaneously by the three satellites of Swarm constellation at two different altitudes (~470 km Swarm A and C; ~520 km Swarm B). In detail, we consider the horizontal component of the magnetic field intensity in the NEC (North-East-Centre) frame (according to ESA nomenclature we use $SW\_OPER\_MAGx\_LR\_1B(x = A, B, C)$ with file counter equal to 0405 and 0406). Our primary interest lies in the horizontal intensity of the magnetic field because we want to study the changes in the scaling features of magnetic fluctuations at high latitudes in the Northern Hemisphere where the magnetic field is nearly vertical and the horizontal component is generally related to high-latitude current systems.

To isolate the external field contribution, the internal field is removed using CHAOS-5 model. It is a high-resolution geomagnetic model which spans a period between 1997 and 2015, and it is obtained considering satellite magnetic data (Swarm, CHAMP, and Ørsted) along with ground observatory data (Finlay et al. 2015). It permits us to analyse directly the horizontal magnetic field of magnetospheric and ionospheric origin and to estimate the spatio-temporal variations of the geomagnetic field due to the occurrence of a geomagnetic storm.

Figure 1 shows the original X and Y component of the geomagnetic field (called X_{Total} and Y_{Total}, respectively) used to evaluate the intensity of the horizontal magnetic field component ($H_{\mathrm{Total}} = (X^2_{\mathrm{Total}} + Y^2_{\mathrm{Total}})^{1/2}$), and the same components obtained after the removal of the internal field generated by CHAOS-5 model (called X_{External} and Y_{External}, respectively) in the selected time interval for Swarm A satellite.

Figure 2 shows data used in this work, which are the values of the intensities of the magnetic field horizontal component, with 1-s time resolution, recorded by the three Swarm satellites between 13 and 25 March 2015 obtained after the removal of magnetic field's internal contribution. A clear global enhancement of the intensity of the magnetic field horizontal component is observed after the sudden storm commencement (SSC) of St. Patrick's Day storm, at 04:45 UT 17 March 2015. Clearly, different current systems contribute to the observed magnetic field enhancement at the different magnetic latitudes explored by Swarm constellation during its orbit. Indeed, during the main and the recovery phase of St. Patrick's Day storm several intense geomagnetic substorms occurred at high latitudes, as monitored in terms of AE and *Sym-H* indices (see Fig. 4). In what follows, we focus on the time evolution of high-latitude disturbance so to attempt a discussion on the magnetic field fluctuations in relation to some physical processes, such as turbulence.

To discuss the dynamical changes in the geomagnetic field fluctuations in relation to the overall ionospheric polar convection and potential structures as recorded using SuperDARN data, obtained results are presented in terms of AACGM latitude (Shepherd 2014) and magnetic local time (MLT) based on the AACGM coordinates (Baker and Wing 1989). In detail, MLT is evaluated using the common definition given by Baker and Wing (1989) according to which $MLT = AACGMLong/15 + const + UT$ where AACGM Long is the magnetic longitude in AACGM coordinates of the point of interest, UT is the universal time that is given in hours and the constant value ($const = -4.73$) has been obtained choosing as standard reference point 0°N, 0°E in geographic coordinates. This coordinate system has been developed to compare measurements coming from different SuperDARN radars, but nowadays it is usually used to map measurements from satellites and/or ground-based instruments to analyse better those plasma and electromagnetic processes characterising the ionosphere and the magnetosphere. It is undefined in a band of ~15° around the magnetic equator but provides

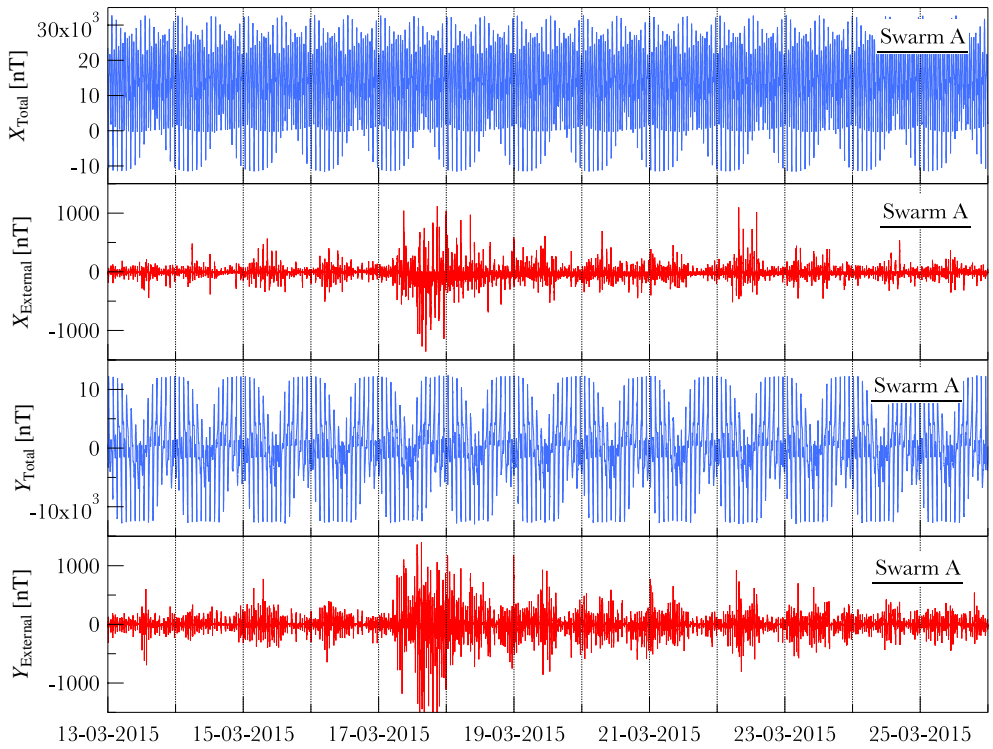

Fig. 1 Total (internal and external) and external magnetic field. Comparison between the original *X* and *Y* component of the geomagnetic field (called X_{Total} and Y_{Total}, respectively) and the temporal trend of the same components obtained after the removal of the geomagnetic field's internal component generated by CHAOS-5 model (called $X_{External}$ and $Y_{External}$, respectively)

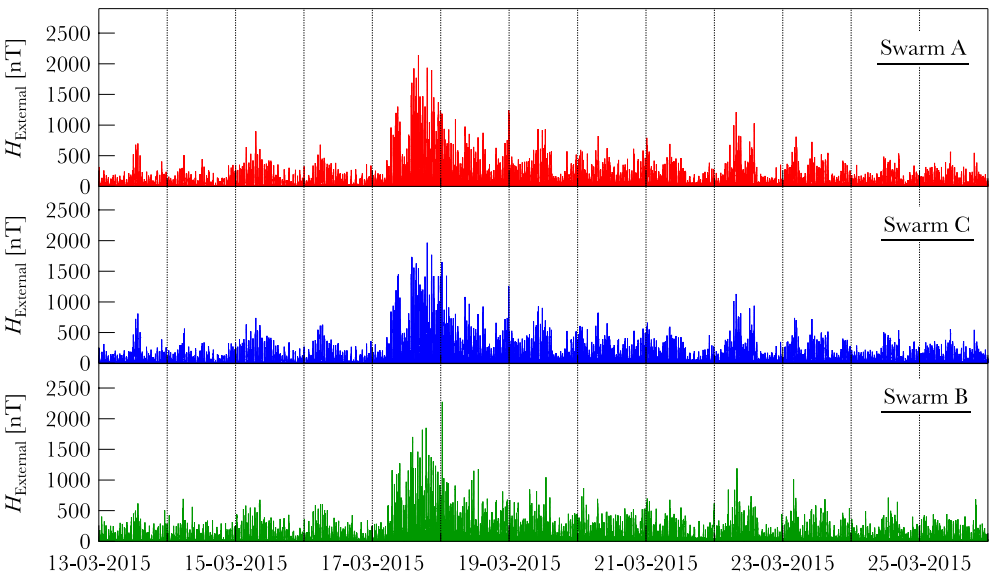

Fig. 2 Work's dataset. (*first* to *third panel*) Horizontal intensities of the Earth's magnetic field recorded by the three Swarm satellites (Swarm *A*, *C* and *B*) between 13 and 25 March 2015 obtained after the removal of magnetic field's internal contribution

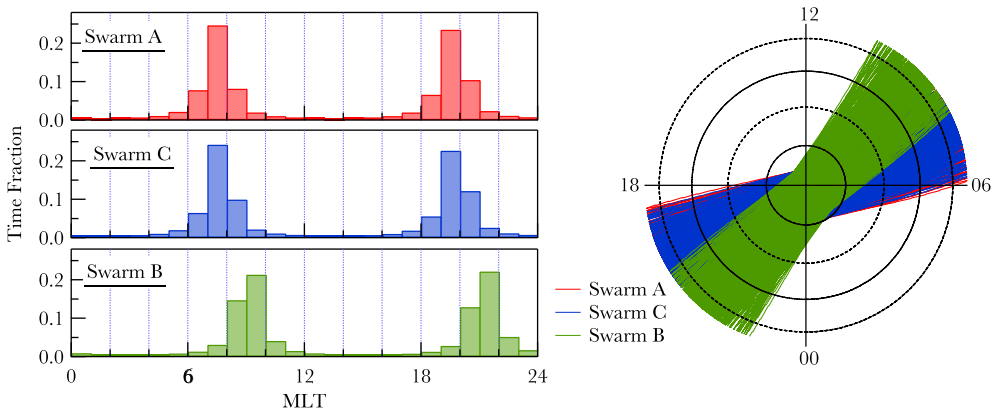

Fig. 3 Trajectories. On the *left*, the time fraction that each satellite spends in the different magnetic local times during the time interval 13–25 March 2015. On the *right*, a polar view map of the three satellite trajectories in the Northern Hemisphere in the same time interval. The coordinates are AACGM latitude, from 50°N to the north pole, and the magnetic local time (MLT), with the local noon at the *top* and local midnight at the *bottom*. *Concentric circles* are magnetic parallels drown at 10°

a good magnetic coordinate representation in the auroral and polar regions which are the regions considered in our study. Software used to transform geographic coordinates into AACGM ones is available at http://engineering.dartmouth.edu/superdarn/aacgm.html. Taking into account the MLT definition, during the analysed period the Swarm satellites span two different magnetic local time intervals (07:00–09:00 MLT and 19:00–21:00 MLT) as it is possible to notice looking at Fig. 3 where a polar view map of the three satellite trajectories in the Northern Hemisphere is reported together with the distributions of magnetic local time for each satellite during its orbit around the Earth.

To describe the space weather conditions during the St. Patrick's Day geomagnetic storm, we consider data relative to interplanetary magnetic field and solar wind plasma (speed, pressure and proton density) with 1-min time resolution recorded by ACE satellite and obtained from the OMNI website (www.cdaweb.gsfc.nasa.gov/istp_public/) that reports data propagated to the front of the magnetosphere. These data are reported together with the geomagnetic indices *Sym-H* and AE in Fig. 4. Looking at the interplanetary magnetic field and plasma parameters, it is evident how the SSC (sudden storm commencement) and the main phase of the geomagnetic storm are strongly related to the sharp increase in the solar wind plasma dynamic pressure and the large rotation of the B_z component of the interplanetary magnetic field. Correspondently, the values of the AE index indicate an increase in the high-latitude geomagnetic activity suggesting an enhancement of the intensity of the auroral electrojet current systems, which persists for some days during the recovery phase of the magnetic storm.

Method of analysis

We are interested in the analysis of the scaling features of geomagnetic field fluctuations at temporal scales shorter than 40 s. We limit our analysis to the range of scales from 1 to 40 s in order to investigate scaling features on at least 1 order of magnitude and simultaneously get local spatial information of the fluctuation field. Moreover, considering the velocity (about 7.6 km/s) of the Swarm satellites and assuming that the evolution time of spatial structures is longer than the transit time, the temporal scales below 40 s roughly correspond to investigate spatial fluctuations from 7.6 km up to $\sim$ 300 km. The link between temporal and spatial scale, i.e. the validity of Taylor's hypothesis according to which the temporal variations of spatial structures can be ignored during the motion of the satellite, has been checked using Swarm A and C satellites which orbit side by side at a distance of about 160 km. Magnetic data coming from the two satellites show the same fluctuation field structure taking into account of the different transit time (about 10 seconds) of the two satellites in the same region. Furthermore, we assume that the magnetic field fluctuations that we are analysing reflect the features of electrojets or mesoscale magnetic structures that evolve on a time scale longer than transit time. In this case, these structures can be supposed relatively stationary and consequently they can be treated as spatial magnetic fluctuations rather than temporal ones.

For our investigation, we evaluate the local Hurst exponent ($\mathcal{H}$), which can be used as an indicator of the state of randomness of a time series. It ranges between 0 and 1 and measures three types of behaviour in a time series: persistence, randomness, and anti-persistence. When the process is a Brownian motion $\mathcal{H}$ is 0.5, when it is

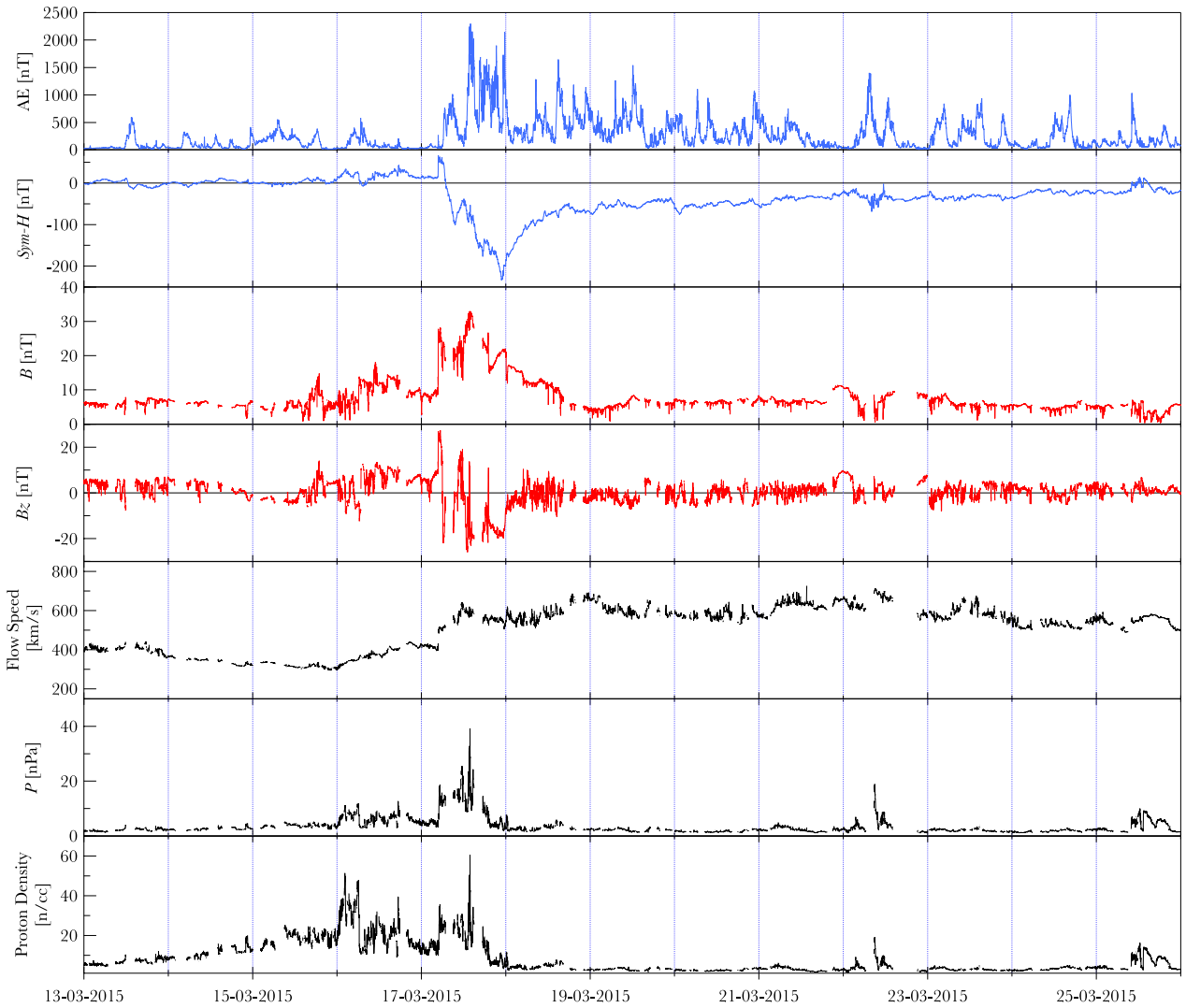

Fig. 4 Geophysical and interplanetary parameters in the analysed period. Variations of geomagnetic activity indices, interplanetary magnetic field (IMF) and solar wind parameter for the analysed time interval (13–25 March 2015). (*First* to *sixth panel*) High-latitude auroral electrojet index AE, low-latitude index *Sym-H*, IMF magnitude *B*, north–south component of IMF B_z, solar wind speed *v*, dynamical pressure *P* and proton density

persistent (i.e. an increment will be followed by a decrement and vice versa) $\mathcal{H}$ is greater than 0.5, and finally when it is anti-persistent (i.e. an increment will be followed by an increment, and a decrement by a decrement) $\mathcal{H}$ is less than 0.5. For a white noise $\mathcal{H} = 0$, while for a simple linear trend, $\mathcal{H}$ is 1. Furthermore, in the case of monoscaling signals a simple relation exists between the Hurst exponent and the spectral density slope β, which is expected to be $\beta = 2\mathcal{H} + 1$ (Gilmore et al. 2002).

A variety of methods exist for estimating the Hurst exponent, and each of them has specific advantages and disadvantages. The most popular methods used to estimate the Hurst exponent are the R/S analysis (rescaled range method) introduced by Mandelbrot (1971), Mandelbrot (1972), the detrended fluctuation analysis (DFA) originally suggested by Peng (1994) and wavelet-based estimation. Here, we employ an alternative method based on the detrended first-order structure function $S_1(\tau)$, which for a signal $x(t)$ defined over an interval T is given by

$$S_1(\tau) = \langle \mid x(t+\tau) - x(t) \mid \rangle_T, \tag{1}$$

where τ is a time separation and $\langle \ldots \rangle_T$ indicates time averaging over the interval T. When we deal with a scale-invariant signal $x(t)$, $S_1(\tau)$ exhibits a power law behaviour as a function of τ

$$S_1(\tau) \sim \tau^{\mathcal{H}} \tag{2}$$

where $\mathcal{H}$ is the Hurst exponent (Gilmore et al. 2002).

In this work, we consider a moving window of 400 s [i.e. $T = 400$ s]. The choice of a moving window of 400 s, which is 10 times larger than the maximum scale τ which we want to investigate (40 s), permits us to have a reliable estimation of 40 s fluctuation statistics.

In the selected time interval, we detrend the time series (H_{External}) by computing the average long-term trend using a seventh-order polynomial fit $p(t)$. In this way, we can construct a new detrended time series $x(t)$,

$$x(t) = H_{\text{External}}(t) - p(t), \quad \forall t \in [t_0 - T/2, t_0 + T/2], \tag{3}$$

to which we apply the structure function analysis. Detrending operation is necessary to obtain a more correct estimation of the Hurst exponent eliminating possible spurious effects due to the contribution from long-range trend. This operation is commonly used to estimate the Hurst exponent in several methods [see also detrending moving average (DMA) and detrended fluctuation analysis (DFA)].

The typical relative error associated with the local Hurst exponent estimated using this method is equal to 4 % with a 95 % confidence according to a Monte Carlo simulation as reported in our previous work (De Michelis et al. 2015).

Results and discussion

We evaluate the local Hurst exponent for three time series consisting of the intensity of the horizontal component of the Earth's magnetic field of external origin recorded by the three satellites of Swarm constellation from 13 to 25 March 2015 (see Fig. 2). Successively, we divide the selected time interval into windows of 1 day and for each window we estimate the average values of the local Hurst exponent obtained considering simultaneously Swarm A, B and C observations during their crossings of the Northern Hemisphere. Thus, the results from each 1 day window come in averaging 45 crossings (15 crossings per day per each satellite). In Fig. 5, the average $\mathcal{H}$ values are plotted as a function of the AACGM latitude along the mean trajectory of the satellite moving from the morning (from 20°N to 90°N AACGM Lat on the left side of Fig. 5 corresponding to 07:00–09:00 MLT interval) to the evening side (from 90°N to 20°N AACGM Lat on the right side of Fig. 5 corresponding to 18:00–20:00 MLT interval). The graphs reported in Fig. 5 give us the opportunity to localise different latitudinal structures caused by different physical processes and to study their time evolution throughout all the phases of the St. Patrick's Day geomagnetic storm. As can be seen from the figure, the analysed time series are characterised by values of the local Hurst exponent both less than and greater than 0.5. This means that the processes responsible for magnetic fluctuations of external origin at scales below 40 s can induce both stability and instability in the system. When the value of the Hurst exponent is less than 0.5 (red in Fig. 5), the magnetic fluctuations are characterised by a correlation with an anti-persistent character. When the value of the Hurst exponent is higher than 0.5 (blue in Fig. 5), the correlations in the magnetic field fluctuations have a persistent character. From the graphs reported in Fig. 5, we can see that, in the analysed time interval, at low and mid-latitudes (<50°N AACGM Lat) the magnetic field fluctuations at scales below 40 s have always a persistent character regardless of the geomagnetic activity level. On the contrary, at very high latitudes (>80°N AACGM Lat), the correlations in the magnetic field fluctuations have an anti-persistent character and the size of this region changes with the geomagnetic activity level. Indeed, we find a well defined region of anti-persistent character around 80°N AACGM Lat during the whole recovery phase of the geomagnetic storm (from 18 to 25 March), while the width of this anti-persistent region becomes larger during both the main phase of the geomagnetic storm (17 March) and the day before (16 March 2015). What is interesting in these data is that the profile of the average values of the local Hurst exponent as function of the AACGM latitude is mainly the same in all days taken into account except for the 16 and 17 March 2015. These 2 days, with respect to all other days here considered, are characterised by an increase in the dynamical pressure of the solar wind along with rapid southward excursions of the IMF B_z component. These features of the solar wind and in particular the enhancement of the solar wind pressure seem to reflect in the decrease in the mean Hurst exponent observed especially on March 16, thus affecting the character of the magnetic field fluctuations. What changes, during the selected period, is essentially the position of the profile of the local Hurst values with respect to $\mathcal{H} = 0.5$. It drops lightly respect to this reference position during the recovery phase of the geomagnetic storm. Moreover, it is apparent that the values of the local Hurst exponent are higher in the evening side (on the right of Fig. 5) than in morning one (on the left of the same figure) at mid–high latitudes (60°–80°). A comparison of the local Hurst exponent values between 60° and 80° in the two different MLT sectors shows clearly this feature except for 16 and 17 March 2015. Indeed, at mid–high latitudes during the recovery phase of the geomagnetic storm $\mathcal{H}$ values are slightly greater than or less than 0.5 in the morning side, while in the evening one they are always characterised by values greater than 0.5.

To better visualise the different latitudinal structures at high latitudes, we report on Fig. 6 polar view maps (AACGM Lat >50°N) of the local Hurst exponent values for the restricted time interval 14–22 March. Each

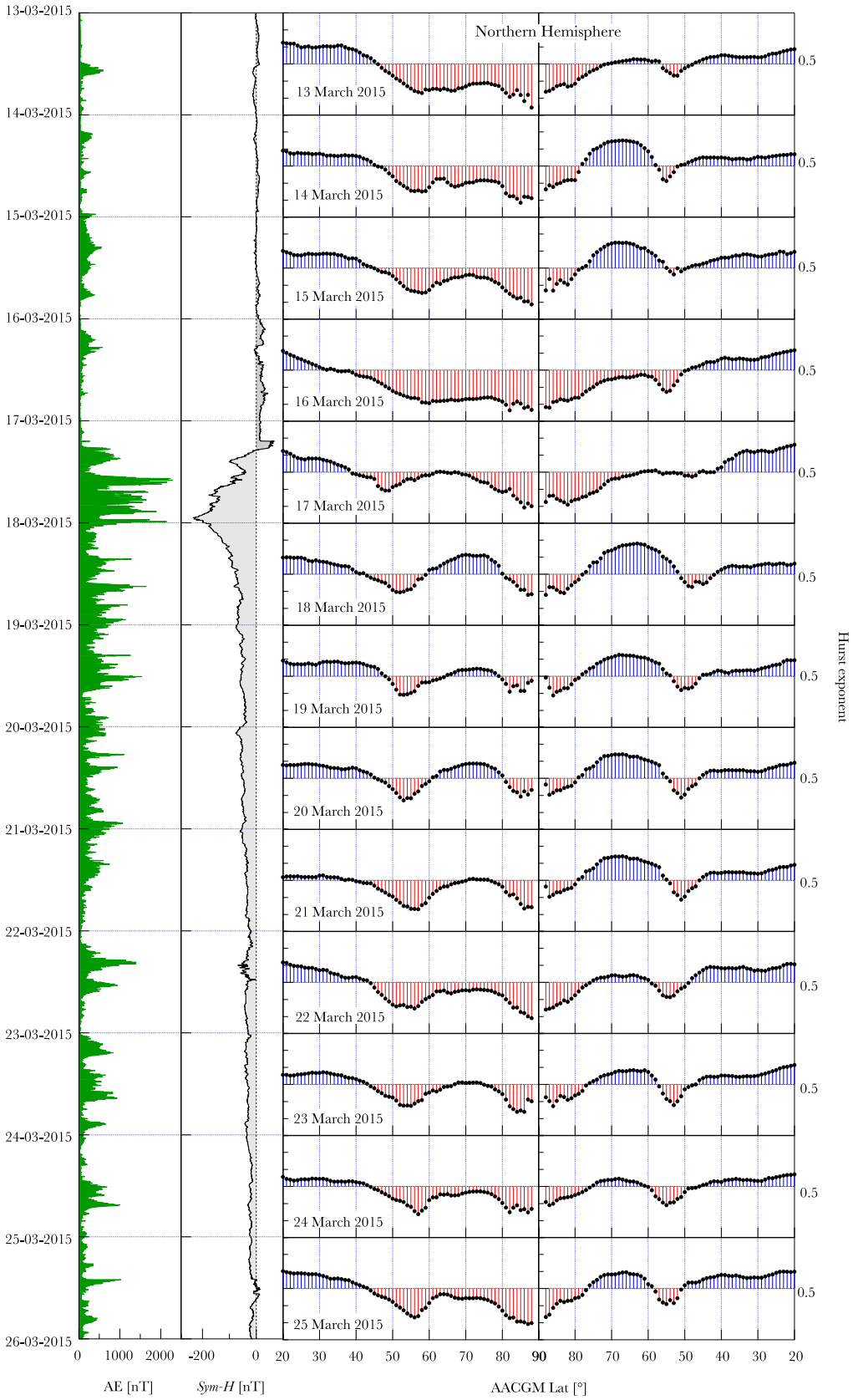
Northern Hemisphere
13 March 2015
14 March 2015
15 March 2015
16 March 2015
17 March 2015
18 March 2015
19 March 2015
20 March 2015
21 March 2015
22 March 2015
23 March 2015
24 March 2015
25 March 2015
13-03-2015
14-03-2015
15-03-2015
16-03-2015
17-03-2015
18-03-2015
19-03-2015
20-03-2015
21-03-2015
22-03-2015
23-03-2015
24-03-2015
25-03-2015
26-03-2015
0.5
Hurst exponent
0 1000 2000
AE [nT]
-200 0
Sym-H [nT]
20 30 40 50 60 70 80 90 80 70 60 50 40 30 20
AACGM Lat [°]

(see figure on previous page.)
Fig. 5 Hurst exponent average latitude profile. (from the *left* to the *right*) Temporal trends of AE and *Sym-H* indices in the time interval 13 and 25 March 2015. Daily profiles of the Hurst exponent values obtained averaging the results coming from the three Swarm satellites as a function of the AACGM latitude moving along the mean trajectory of the satellite from the morning (on the *left*) to the evening side (on the *right*)

panel represents the local Hurst exponent values relative to 1 day obtained considering the measurements coming from the three Swarm satellites orbiting the regions of interest during the selected day. To compute these maps, data are reduced on a regular grid using a Gaussian kernel interpolation scheme. As in Fig. 5, the magnetic field fluctuations with an anti-persistent character are shown in red, while those with a persistent character are reported in blue. On each image, we also report the temporal trend of the auroral electrojet (AE) index for the selected day using the same amplitude scale (0–2500 nT) in all the images. The AE index values show an intense global electrojet activity in the auroral zone during both the main phase and the recovery phase of the St. Patrick's Day storm. Thus, during the recovery phase of the geomagnetic storm (from 18 to 22 March) the auroral region, as monitored in terms of the AE index, is characterised by an intense substorm activity. An interesting result emerging from Fig. 6 is the change in the morning–evening asymmetry of the $\mathcal{H}$ exponent values from quiet to disturbed periods. During periods characterised by a low geomagnetic activity (14, 15, 16, 21 and 22 March), we observe a marked asymmetry, while this is reduced during periods characterised by a high substorm activity (from 17 to 20 March 2015).

The morning–evening asymmetry of the $\mathcal{H}$ exponent values observed during quiet periods may reflect the different turbulent character of fluctuations, characterised by different spectral features. Indeed, considering the distribution of the Hurst exponent values the slope of the power spectral density of magnetic fluctuations ($\mathcal{H} < 0.5$; $\beta < 2$) is flatter in the morning side than in the evening one ($\mathcal{H} > 0.5$; $\beta > 2$). In the morning side where the magnetic field's fluctuations have an anti-persistent character and the magnetic field's spectral density is characterised by an exponent smaller than 2, the field fluctuation shows the formation of small structures. In the evening side where the magnetic field's spectrum is steeper, the formation of small structures is reduced. The different spectral features reflect a different origin of the turbulent fluctuations: shear flow in the evening side, gradient drift or current convective in the morning side. The asymmetry in the particle precipitation could play a role in the different turbulent character. This point requires more investigation and will be explored in a further work.

Besides the morning–evening asymmetry, the most interesting finding reported in Figs. 5 and 6 is the significant change in the values of the local Hurst exponent during the development of the geomagnetic storm. The polar view maps show a decrease in the local Hurst exponent values at all high magnetic latitudes approaching and during the main phase of the geomagnetic storm suggesting a change in the scaling features of the geomagnetic field fluctuations from a more persistent to a less persistent pattern. These results are consistent with those of De Michelis and Consolini (2015) who have analysed the spatial distribution of the scaling features of the magnetic field fluctuations at scales below 100 min using data coming from 45 ground-based geomagnetic observatories distributed in the Northern Hemisphere. This means that the change in the nature of the geomagnetic field fluctuations, which is a consequence of dynamical processes that are activated during disturbed periods, occurs on a wide spectrum of spatio-temporal scales since similar results are obtained analysing the scaling features of magnetic field fluctuations below both 40 s and 100 min.

From the polar maps in Fig. 6, it is apparent that there are some features of the spatial distribution of the local Hurst exponent values that must be investigated. For example, the anti-persistent region around the geomagnetic pole and the presence at high latitudes of regions with persistent magnetic fluctuations visible during the recovery phase of the geomagnetic storm.

To try to understand the nature of these dynamical structures manifesting in the persistency of fluctuations and their time evolution, we compare them with the observations of the global ionospheric convection pattern determined by the Super Dual Auroral Radar Network (SuperDARN). This network is made up of high-frequency (8–20 MHz) coherent scatter radars that emit a series of radio wave pulses transmitted in a beam directed forward of the antenna arrays. Measuring the Doppler shift between the emitted signal and the reflected one, it is possible to measure the velocity of the ionospheric convection flow in the radar look direction over the polar regions and to have information on the decameter-scale plasma irregularities in the E and F regions of the ionosphere. Combining the line-of-sight vectors obtained from different radars with overlapping fields of view, the radar observations are capable of providing a coverage over a large area giving a comprehensive view of the plasma motion in the polar ionosphere.

A number of techniques have been developed in order to obtain 2-D plasma flow vectors; here we use the "map potential" model developed by Ruohoniemi and Baker (1998) where the measurements from all the SuperDARN

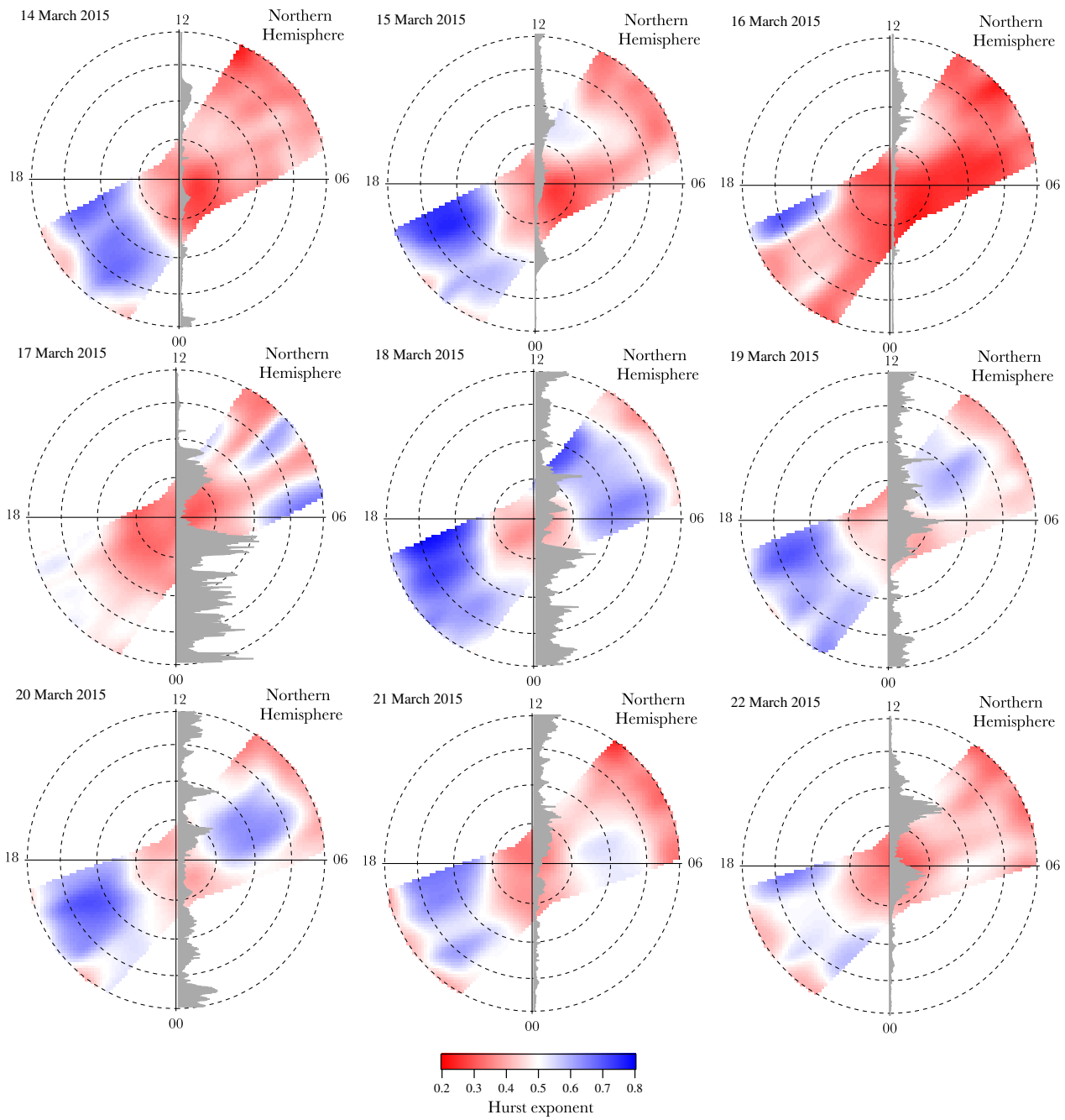

Fig. 6 Polar view maps. Polar view maps of the local Hurst exponent values in the Northern Hemisphere for the time interval 14–22 March 2015. The coordinates are AACGM latitude, from 50°N to the north pole, and the magnetic local time (MLT), with the local noon at the *top* and local midnight at the *bottom*. *Concentric circles* are magnetic parallels drown at 10°. On each map, the temporal trend of AE index for the corresponding day is reported using the same scale in all the *graphs*

radars are combined with data from a statistical model (Ruohoniemi and Greenwald 1996) to produce a convection pattern over the entire convection zone that is in best agreement with the line-of-site velocity measurements provided by the SuperDARN radars. SuperDARN radars can operate in different modes changing the frequency or the time resolution for the purpose of achieving specific research goals. In the standard mode of operation, each radar measures the line-of-sight plasma velocity at 75 ranges along each of 16 beam directions

covering an area of about 3500 km in range and about 56 degrees in azimuth. Using this normal operating mode, global convection maps based on SuperDARN measurements are available at 2-min intervals.

To compare the global convection pattern obtained in the Northern Hemisphere using SuperDARN data with the results obtained using Swarm measurements, we have to consider for each day the time intervals where all the three satellites are simultaneously at high latitude (>50°N AACGM Lat). Unfortunately, this particular configuration does not occur frequently. Indeed, while the Swarm A and C orbit side by side at an altitude of about 470 km, the third satellite (Swarm B), which maintains an altitude of 530 km, flies along an orbit that has an inclination angle with respect to that of the lower pair of satellites which correspond to a magnetic local time separation of about 2 h during the analysed time interval. This different configuration of the Swarm satellites is responsible of the different time periods in which the satellites fly over the northern polar region. Figure 7 shows the difference between the latitudinal values spanned by the two satellites Swarm B and Swarm C during their trajectories in the analysed period. As can be seen from the figure, there is only one time interval during which the three satellites move on the polar region simultaneously covering an area of about 40° in the Northern Hemisphere. This time interval, which corresponds to a latitudinal difference value near to zero, occurs on 15 March from 18:32 UT to 18:52 UT. In the other time interval characterised by a latitudinal value near to zero, the three satellites are simultaneously in the Southern Hemisphere. So, to compare Swarm outcomes with SuperDARN data in the Northern Hemisphere, we have to consider also other time intervals when there is not a simultaneous complete coverage of the polar region by the whole Swarm constellation.

Figure 8 compares the average global ionospheric convection pattern obtained using SuperDARN data during the time interval of about 20 min that the satellites take to cross the high-latitude region (> 50° N AACGM Lat) and the local Hurst exponent values evaluated using data coming from the single crossings of satellites.

It is known that at high-latitude, configuration of the plasma convection in the ionosphere follows regular patterns, which are mainly dependent on the orientation and strength of the IMF and which vary in extension with the strength of solar wind interaction. Indeed, reconfigurations of ionospheric convection pattern can occur as a consequence of sudden changes in the polarity of the B_z and B_y components of the IMF. This is the reason why the ionospheric convection on timescales of minutes can be quite variable, even for relatively stable IMF conditions (Bristow et al. 2004; Huang et al. 2000a, b). However, if the configuration of the ionospheric plasma convection is well established during those periods in which the IMF is southward, when the IMF is northward the situation is more complicated, and the transformation of the ionospheric convection pattern during a sudden change in the orientation of the IMF is not well known. This complex configuration of the horizontal circulation streamlines can be noted looking at the SuperDARN image reported in Fig. 8 where various scenarios are depicted. Some images are characterised by a double-celled convection pattern with the dawn cell dominant on the dusk one for a southward B_z (Fig. 8c, d and f), some have a more complex convection pattern which consists of several cells for northward B_z (Fig. 8a and e) and lastly in some others the cells merge into one large near-corotation cell (Fig. 8b). Since all these typical features of the horizontal circulation streamlines are due to the interaction between the IMF and the Earth's magnetosphere, these convection patterns can be considered

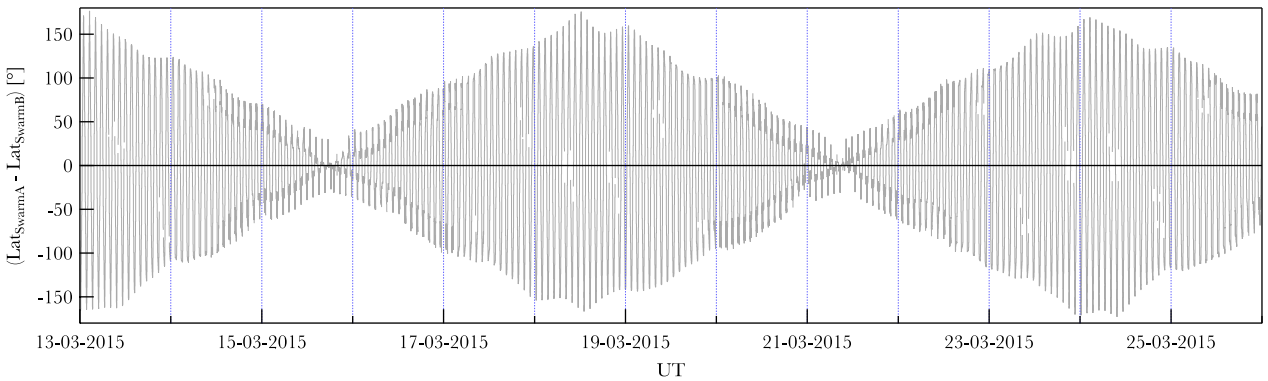

Fig. 7 Latitudinal difference between Swarm satellites. Difference between the latitudinal values spanned by the two satellites Swarm B and Swarm C during their trajectories in the period 13–25 March 2015

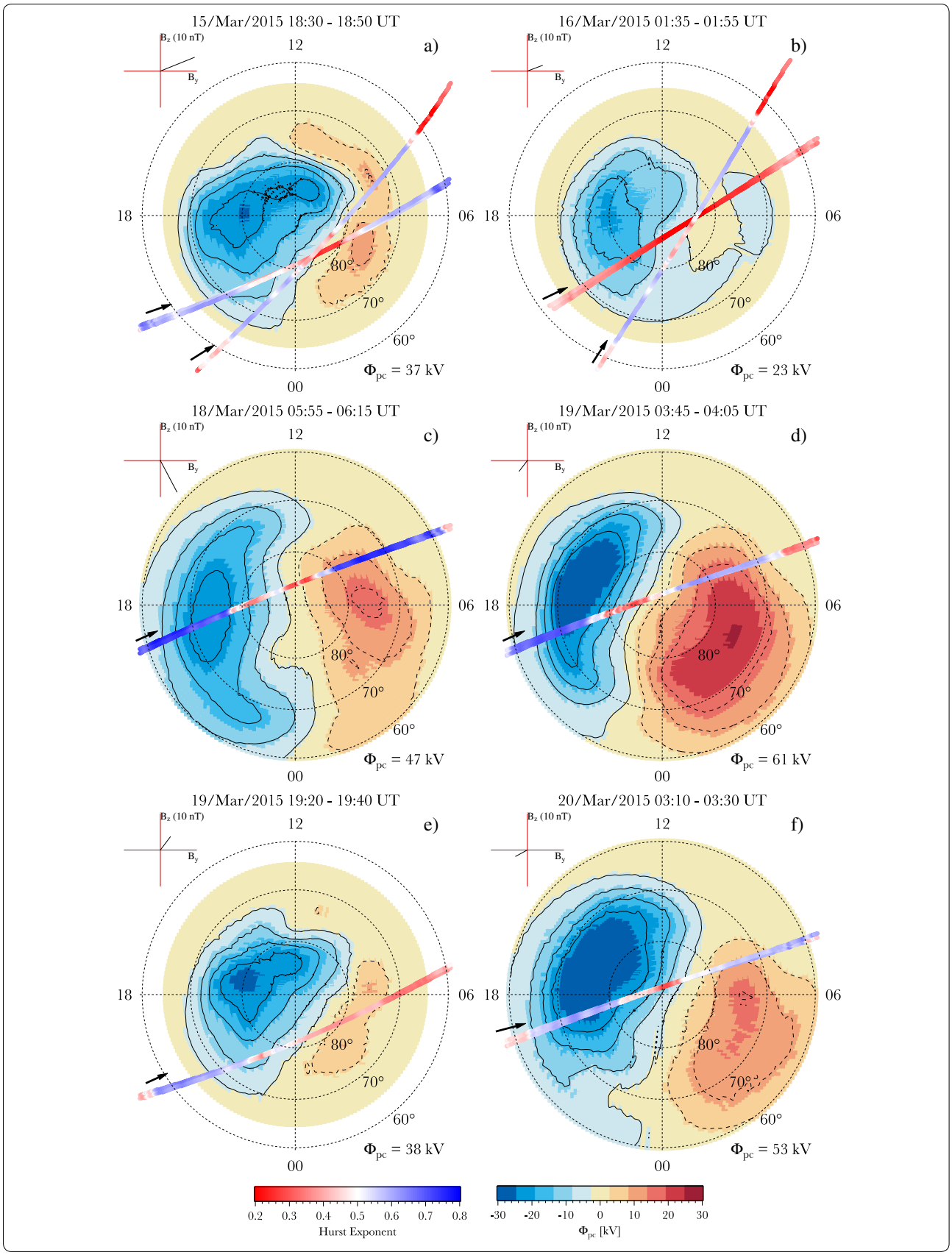
15/Mar/2015 18:30 - 18:50 UT
a)
B_z (10 nT)
B_y
12
18
06
00
80°
70°
60°
Φ_{pc} = 37 kV
16/Mar/2015 01:35 - 01:55 UT
b)
Φ_{pc} = 23 kV
18/Mar/2015 05:55 - 06:15 UT
c)
Φ_{pc} = 47 kV
19/Mar/2015 03:45 - 04:05 UT
d)
Φ_{pc} = 61 kV
19/Mar/2015 19:20 - 19:40 UT
e)
Φ_{pc} = 38 kV
20/Mar/2015 03:10 - 03:30 UT
f)
Φ_{pc} = 53 kV
0.2 0.3 0.4 0.5 0.6 0.7 0.8
Hurst Exponent
-30 -20 -10 0 10 20 30
Φ_{pc} [kV]

(see figure on previous page.)
Fig. 8 Comparison between SuperDARN and Swarm constellation measurements. Mean ionospheric plasma convection maps in the high-latitude region obtained using SuperDARN data. *Colour* indicates electrostatic potential according to the colour scale at the *bottom*. Superposed to the mean ionospheric plasma convection maps the values of the Hurst exponent along the trajectories of the Swarm satellites. **a**–**f** Different time intervals as reported at the *top* of *each panel*. The coordinates are AACGM latitude, from 60°N to the north pole, and the magnetic local time (MLT), with the local noon at the *top* and local midnight at the *bottom*. *Concentric circles* are magnetic parallels drown at 10°

as indicators of the state of the coupled magnetosphere–ionosphere system (Ruohoniemi and Greenwald 1996).

The local Hurst exponent values reported on each image of Fig. 8 suggest that the values of $\mathcal{H}$ higher than 0.5 (blue) occur in those regions characterised by strong double-celled convection pattern. When this happens, the transition of the local Hurst exponent to values smaller than 0.5 can be observed, in first approximation, near the border of the convection region (Heppner–Maynard boundary) in proximity of the location of the auroral oval. There is also a sharp transition to values smaller than 0.5 between the two-cell pattern in the polar cap. We deduce that in periods with an intense substorm activity and characterised by persistent double-celled convection patterns, the plasma dynamics is capable of generating a long-range dependence in the magnetic field fluctuations. This cannot be established when the polar convection patterns quickly change. Indeed, when the southward B_z varies from negative to positive, the horizontal circulation streamlines flowing within the polar cap change in intensity and orientation. The distribution of the flow within the polar cap is anti-sunward and peaked near the noon-midnight meridian for negative B_z, it reverses for positive B_z (the so-called reversed convection) (Maezawa 1976; Crooker 1992; Burke et al. 1979). In this condition, the polar cap can be characterised by non-uniformities which are responsible for the development of strong shears in the flow.

An interesting correlation seems to exist also with the value of the polar cap potential ϕ_{PC}. Indeed, for high values of ϕ_{PC} and negative values of the IMF B_z component (see for instance plate (d) and (f) in Fig. 8) a clear structure of the magnetic field fluctuations character is found in coincidence with the occurrence of a stable double-celled convection pattern. Conversely, for small values of ϕ_{PC} and/or positive values of IMF B_z component, the highly structured character of the magnetic field fluctuations is lost. This last observation is supported by Fig. 8b when a single cell is found with $B_z > 0$ and $\phi_{PC} < 20$ kV.

Summary and conclusions

The purpose of the current study is to investigate the possibility to utilise the spatial changes in the scaling properties of the geomagnetic field's fluctuations as a local indicator of the overall magnetosphere–ionosphere coupling conditions and of the plasma convection structures during geomagnetic storms. For this reason, we have analysed the changes in the scaling properties of the geomagnetic field's fluctuations recorded at high latitude by the Swarm constellation.

We have evaluated the local Hurst exponent of the horizontal intensity of the Earth's magnetic field recorded by the three Swarm satellites from 13 to 25 March 2015 obtained after the removal of magnetic field's internal contribution evaluated using CHAOS-5 model. In this way, we have locally measured the degree of persistence or anti-persistence of the external magnetic field's fluctuations. We have assumed that the temporal variations of spatial structures can be ignored (Taylor hypothesis) during the motion of the satellites. Therefore, we have analysed magnetic fluctuations below 40 s being interested in the local spatial feature below 300 km.

The question of the nature of the spatio-temporal fluctuations at high latitudes has been addressed in several previous studies (Kintner and Seyler 1985; Weimer et al. 1985; Golovchanskaya et al. 2006; Golovchanskaya and Kozelov 2010). Different techniques and different physical quantities describing the magnetosphere–ionosphere system (electric and magnetic field, ionospheric plasma velocity and so on) have been used to try to understand the fluctuation properties that occur on both closed magnetic field lines (in the auroral zone) and open ones (in the polar cap). The idea behind is to comprehend if the properties of the fluctuations that occur in areas of open magnetic field topology are directly driven by the solar wind and are characterised by different properties with respect to areas of closed magnetic field topology.

In the current study, we indirectly address this question investigating the scaling properties of the magnetic field fluctuations at high latitude and their time evolution throughout all the phases of the St. Patrick's Day storm. During the selected period, as monitored in terms of the AE index, several intense magnetic substorms occurred at high latitude during all the different geomagnetic storm phases. It is known that the magnetic field fluctuations associated with large spatial scales (>1000 km) are caused at low and mid-latitudes mainly by the magnetospheric ring current as well as by the outlying effects of the polar electrojets, and at high latitudes (i.e. at auroral and polar cap latitudes) by that complex

system of electric currents which usually comprises the polar electrojets, an electric current flowing in the polar cap and the sheets of field-aligned currents flowing from and to the magnetosphere. These large-scale fluctuations are well studied and are found to depend on different parameters such as the interplanetary magnetic field, the solar wind density and velocity and the season. Conversely, the magnetic field fluctuations associated with small spatial scales (<100 km) remain the subject of much investigation.

The detailed analysis of the selected period permits us to investigate the effect of the storm and substorms on the magnetic field's fluctuations and to address the spatial and temporal evolution of the mesoscale fluctuations and their dependence on interplanetary and geomagnetic parameters. Our results show that: (a) during geomagnetically quiet period (13, 14 and 15 March) the magnetic field's fluctuations have a persistent character in the evening side while they are characterised by a less persistent character in the morning one; (b) during the main phase of the storm (17 March) and the day before (16 March) the geomagnetic field's fluctuations change from a more to less persistent character; (c) during the recovery phase of the storm intense geomagnetic substorms occur when the magnetic field's fluctuations assume a persistent behaviour mainly in the auroral zone both in the morning and in the evening sectors.

Taking into account that for a scale-invariant signal there exists a direct relationship between the values of the Hurst exponent and of the exponent β of the power spectral density ($\beta = 2\mathcal{H} + 1$) (Gilmore et al. 2002), our findings suggest that the regions where the magnetic field's fluctuations have a persistent character correspond to regions where the geomagnetic field's spectral density is characterised by an exponent greater than 2. Conversely, when the magnetic field's fluctuations have an anti-persistent character, the geomagnetic field's spectral density has an exponent less than 2. Considering that it has been found that the small-scale variations in the magnetic and electric fields are generally intermittently turbulent, our findings suggest that distinct turbulent regimes characterised the mesoscale magnetic field's fluctuations and that some factors, which are known to influence large-scale fluctuations, have also an influence on mesoscale fluctuations. The results reported in Fig. 6 show that the scaling properties of the geomagnetic field's fluctuations are influenced by geomagnetic activity as monitored by the AE and *Sym-H* and by interplanetary parameters. Furthermore, the comparison between the local Hurst exponent values along a single crossing of polar region and the corresponding average structure of global convection and polar cap potential as reconstructed using data from the SuperDARN (see Fig. 8) shows that gradients or shears in the background plasma drift can influence the nature of the magnetic field's fluctuations. This suggests that plasma instabilities and gradients in the conductance can be a possible source of the observed different nature in the turbulence. Indeed, it possible to notice that: a) the structures of double-celled convection pattern are usually associated with those regions with a more persistent behaviour of the short timescale fluctuations and b) in the polar cap at latitudinal values above 80° N the magnetic field's fluctuations have an anti-persistent character.

These findings do not support our previous research (De Michelis et al. 2015) where we have found that the scaling properties of the magnetic field's fluctuations are basically the same at high latitudes in the auroral oval and in the polar cap. A possible explanation for this apparent inconsistency might be that in the present study we analyse a single strong geomagnetic event, while in our previous study (De Michelis et al. 2015) we have performed an average analysis based on 6 months (about 3000 crossings) of data without particularly strong magnetic events.

However, the issue of the scale-free structure of the physical quantities describing the processes at high latitudes (as for example the electric and magnetic field or the plasma drift velocity) in regions of both open and closed field lines and the relative power law exponents is still open. It has been found that the scale-free spatial structure of the ionospheric velocity fluctuations measured by the Halley SuperDARN radar between 45 km up to about 1000 km is characterised by different values of power law exponents in areas of open and closed magnetic field lines (Abel et al. 2006, 2007). At the same time, analysing the scaling features of the electric field fluctuations on scales of 0.5–256 km at various altitudes over the auroral zone and polar cap some authors have not found significant differences (Golovchanskaya et al. 2006; Golovchanskaya and Kozelov 2010), suggesting that the drivers of turbulence in the two regions probably have the same nature. The comparison between the different studies is not simple. Beyond the fundamental problem of the different spatial and temporal scales analysed, it is necessary to notice that there is not a one-to-one correspondence between the different physical quantities. For example, the results obtained in the case of the electric field's fluctuations cannot be straightforwardly considered valid for the magnetic field (Weimer et al. 1985). Indeed, it has been shown that the Fourier spectra of the east–west component of the magnetic field (B_y) and of the north–south component of the electric field (E_x) have a similar power laws but that this correspondence is valid only in the auroral zone where the field lines are closed (Weimer et al. 1985). Moreover, the present analysis treats the horizontal component of the magnetic

field and not the single east–west component (Y); consequently, the comparison is even more difficult.

In conclusion, the obtained results are an example of the capability of geomagnetic field fluctuations data to generate new insights on the ionosphere–magnetosphere coupling and, at the same time, to develop new applications using their changes in scaling features as a local indicator of the magnetosphere conditions. Indeed, the good agreement between the structure of global convection obtained from SuperDARN and the time average structures obtained from the Hurst exponent suggests that the knowledge of the changes in the scaling features with the geomagnetic activity level may be also useful in developing reliable forecasting systems, providing information not available in geomagnetic indices and, at the same time, on the spatial long-range statistical nature of the geomagnetic field fluctuations at different latitudes. This information can give new key clues for the development of more actual physical models.

Abbreviations

ESA: European Space Agency; CME: coronal mass ejection; ACE: advanced composition explorer; GPS: global positioning system; NEC: North-East-Centre; CGM: geomagnetic coordinates; AACGM: altitude-adjusted corrected geomagnetic; MLT: magnetic local time; UT: universal time; AE: auroral electrojet index; AU: amplitude upper index; AL: amplitude lower index; PC: polar cap index; Sym-H: longitudinally symmetric disturbance index in the horizontal (dipole pole) direction H; HP: hemispheric power index; ROTI: total electron content index; IMF: interplanetary magnetic field; TEC: total electron content; SuperDARN: super dual auroral radar network; SSC: sudden storm commencement; $\mathcal{H}$: Hurst exponent; ϕ_{PC}: polar cap potential.

Authors' contributions

PDM designed the study, performed analysis and drafted the manuscript; GC developed the methodology and revisited the manuscript for important intellectual content; RT collected Swarm data, synthesised internal field by CHAOS-5 model and drafted the manuscript; MFM collected SuperDARN data and performed the analysis of these data. All authors read and approved the final manuscript.

Author details

[1] Istituto Nazionale di Geofisica e Vulcanologia Roma, Via di Vigna Murata 605, 00143 Rome, Italy. [2] INAF-Istituto di Astrofisica e Planetologia Spaziali, Via Fosso del Cavaliere 100, 00133 Rome, Italy.

Acknowlegements

This work is supported by the Italian National Program for Antarctic Research (PNRA) Research Project 2013/AC3.08. The results presented in this paper rely on data collected by the three satellites of the Swarm constellation and SuperDARN data. We thank the European Space Agency that supports the Swarm mission and the national scientific funding agencies of Australia, Canada, China, France, Italy, Japan, South Africa, UK and USA that funded the radars of the SuperDARN network. The authors also acknowledge the use of the SuperDARN software and web tools made available at Virginia Tech. The authors kindly acknowledge N. Papitashvili and J. King at the National Space Science Data Center of the Goddard Space Flight Center for the use permission of 1-min OMNI data and the NASA CDAWeb team for making these data available. The authors are also grateful to authors of CHAOS-5 model for making it available.

The elaborated data for this paper are available by contacting the corresponding author (paola.demichelis@ingv.it).

Competing interests

The authors declare that they have no competing interests.

Received: 29 January 2016 Accepted: 18 May 2016
Published online: 21 June 2016

References

Abel GA, Freeman MP (2002) A statistical analysis of ionospheric velocity and magnetic field power spectra at the time of pulsed ionospheric flows. J Geophys Res 107:1470. doi:10.1029/2002JA009402

Abel GA, Freeman MP, Chisham G (2006) Spatial structure of ionospheric convection velocities in regions of open and closed magnetic field topology. Geophys Res Lett 33:L24103. doi:10.1029/2006LO027919

Abel GA, Freeman MP, Chisham G, Watkins NW (2007) Investigating turbulent structure of ionospheric plasma velocity using the Halley SuperDARN radar. Nonlinear Process Geophys 14:799

Baker NB, Wing S (1989) A new magnetic coordinate system for conjugate studies at high latitudes. J Geophys Res 94:9139

Bristow WA, Greenwald RA, Shepherd SG, Hughes JM (2004) On the observed variability of the cross-polar cap potential. J Geophys Res 109:A02203. doi :10.1029/2003JA010206

Borovsky JE, Funsten HO (2003) MHD turbulence in the Earth's plasma sheet: dynamics, dissipation, and driving. J Geophys Res. doi:10.1029/2002JA009625

Burke WJ, Kelly MC, Sagalyn RC, Smiddy M, Lai ST (1979) Polar cap electric field structure with a northward interplanetary magnetic field. Geophys Res Lett 6:1

Cherniak I, Zakharenkova I (2015) Dependence of the high-latitude plasma irregularities on the auroral activity indices: a case study of 17 March 2015 geomagnetic storm. Earth Planets Space 67:151

Cherniak I, Zakharenkova I, Redmon RJ (2015) Dynamics of the high-latitude ionospheric irregularities during the 17 March 2015 St. Patrick's Day storm: ground-based GPS measurements. Space Weather 13:585

Consolini G (1997) Sandpile cellular automata and the magnetospheric dynamics, cosmic physics in the year 2000. In: Proceedings of 8th GIFCO conference, SIF, Bologna, 123

Consolini G, Chang TS (2001) Magnetic field topology and criticality in geotail dynamics: relevance to substorm phenomena. Space Sci Rev 95:309

Consolini G, De Michelis P, Meloni A, Cafarella L, Candidi M (1998) Levy-stable probability distribution function of magnetic field fluctuations at Terra Nova Bay (Antarctica). In: Proceedings of Italian Research on Antarctic Atmosphere, 367, Soc. Ital. di Fis., Bologna, Italy

Crooker NU (1992) Reverse convection. J Geophys Res 19:363

De Michelis P, Consolini G (2015) On the local Hurst exponent of geomagnetic field fluctuations: spatial distribution for different geomagnetic activity levels. J Geophys Res Space Phys. doi:10.1002/2014JA020685

De Michelis P, Consolini G, Tozzi R (2015) Magnetic field fluctuation features at Swarm's altitude: a fractal approach. Geophys Res Lett. doi:10.1002/2015GL063603

Dyson PL, McClure JP, Hanson WB (1974) In situ measurements of the spectral characteristics of ionospheric irregularities. J Geophys Res 79:1497

Finlay CC, Olsen N, Toeffner-Clausen L (2015) DTU candidate field models for IGRF-12 and the CHAOS-5 geomagnetic field model. Earth Planets Space 67:114

Forte B, Radicella S (2004) Geometrical control of scintillation indices: what happens for GPS satellites. Radio Sci 39:RS5014

Gilmore M, Rhodes TL, Peebles WA (2002) Investigation of rescaled range analysis, the Hurst exponent, and long-time correlations in plasma turbulence. Phys Plasmas 9:1312

Golovchanskaya IV, Kozelov BV (2010) On the origin of electric turbulence in the polar cap ionosphere. J Geophys Res 115:A09321. doi:10.1029/2009JA014632

Golovchanskaya IV, Ostapenko AA, Kozelov BV (2006) Relationship between the high-latitude electric and magnetic turbulence and the Birkeland field-aligned currents. J Geophys Res 111:A12301. doi:10.1029/2006JA011835

Huang C-S, Murr D, Sofko GJ, Hughes WJ, Moretto T (2000a) Ionospheric convection response to changes of interplanetary magnetic field Bz component during strong By component. J Geophys Res 105:5231
Huang C-S, Sofko GJ, Koustov AV, Andre DA, Ruohoniemi JM, Greenwald RA, Hairston MR (2000b) Evolution of ionospheric multicell convection during northward interplanetary magnetic field with $|Bz/By| > 1$. J Geophys Res 105:27095
Kelley MC, Vickrey JF, Carlson CW, Torbert R (1982) On the origin and spatial extent of high-latitude F-region irregularities. J Geophys Res 87:4469
Kintner PM, Seyler CE (1985) The status of observations and theory of high latitude of ionospheric and magnetospheric plasma turbulence. Space Sci Rev 41:91
Mandelbrot B (1971) When can price be arbitraged efficiently? A limit to the validity of the random walk and martingale models. Rev Econ Stat 53:225
Mandelbrot B (1972) Statistical methodology for nonperiodic cycles from covariance to R/S analysis. Ann Econ Soc Meas 1:259
Maezawa K (1976) Magnetospheric convection induced by the positive and negative Z components of the interplanetary magnetic field: quantitative analysis using polar cap magnetic records. J Geophys Res 81:2289
Nishitani N, Hori T, Kataoka R, Ebihara Y, Shiokawa K (2015) Characteristics of ionospheric convection associated with low-latitude aurora observed at Rikubetsu, Hokkaido during the 2015 March storm, paper presented at SuperDARN workshop 2015, Leicester, UK
Olsen N et al (2013) The Swarm satellite constellation application and research facility (SCARF) and Swarm data products. Earth Planets Space 65:1189
Parkinson ML (2006) Dynamical critical scaling of electric field fluctuations in the greater cusp and magnetotail implied by HF radar observations of F-region Doppler velocity. Ann Geophys 24:689
Peng KC et al (1994) Mosaic organization of DNA nucleotides. Phys Rev E 49:1685
Pi X, Mannucci AJ, Lindqwister UJ, Ho CM (1997) Monitoring of global ionospheric irregularities using the worldwide GPS network. Geophys Res Lett 24:2283
Pulkkinen A, Klimas A, Vassiliadis D, Uritsky V, Tanskanen E (2006) Spatiotemporal scaling properties of the ground geomagnetic field variations. J Geophys Res 111:A03305. doi:10.1029/2005JA011294
Ruohoniemi JM, Baker KB (1998) Large-scale imaging of high-latitude convection with Super Dual Auroral Radar Network HF radar observations. J Geophys Res 103:20797
Ruohoniemi JM, Greenwald RA (1996) Statistical patterns of high-latitude convection obtained from Goose Bay HF radar observations. J Geophys Res 101:21743
Shepherd SG (2014) Altitude-adjusted corrected geomagnetic coordinates: definition and functional approximations. J Geophys Res Space Phys 119:7501
Sitnov MI, Sharma AS, Papadopoulos K, Vassiliadi D (2001) Modeling substorm dynamics of the magnetosphere: from self-organization and self-organized criticality to nonequilibrium phase transitions. Phys Rev E 65:016116
Uritsky VM, Pudovkin MI (1998) Low frequency 1/f like fluctuations of the AE-index as a possible manifestation of self-organized criticality in the magnetosphere. Ann Geophys 16:1580
Weimer D, Goertz C, Gurnett D, Maynard N, Burch J (1985) Auroral-zone electric fields from DE-1 and DE-2 at magnetic conjunctions. J Geophys Res Space Phys 90:7479